Check for updates

Synthesis and comparative study of (NHC$_F$)PdCl$_2$Py and (NHC$_F$)Ni(Cp)Cl complexes: investigation of the electronic properties of NHC ligands and complex characteristics†

Roman O. Pankov,[a] Ignatii R. Tarabrin,[a,b] Alexandra G. Son, [c]
Mikhail E. Minyaev, [a] Darya O. Prima [a] and Valentine P. Ananikov [*a]

The electron-donating and electron-accepting properties of N-heterocyclic carbene (NHC) ligands play a pivotal role in governing their interactions with transition metals, thereby influencing the selectivity and reactivity in catalytic processes. Herein, we report the synthesis of Pd/NHC$_F$ and Ni/NHC$_F$ complexes, wherein the electronic parameters of the NHC ligands were systematically varied. By performing a series of controlled structure modifications, we elucidated the influence of the σ-donor and π-acceptor properties of NHC ligands on interactions with the transition metals Pd and Ni and, consequently, the catalytic behavior of Pd and Ni complexes. The present study deepens our understanding of NHC–metal interactions and provides novel information for the rational design of efficient catalysts for organic synthesis.

Introduction

Three decades after the historic discovery of Arduengo free N-heterocyclic carbenes (NHCs), these compounds have become a staple in the toolkit of catalytic chemists.[1–8] They are used as ligands for various metals in a wide variety of catalytic transformations, competing with previously known phosphine ligands.[9–16] The advantages of the new class of ligands include their high donor capacity, stability, and ability to fine-tune electronic and steric properties.[17–22] The properties of NHC ligands with electron acceptor substituents have been most widely studied for palladium complexes in cross-coupling reactions, ruthenium and rhodium complexes in metathesis reactions and gold complexes in various other transformations.[23–30] In the catalytic cycle of cross-coupling reactions, it has been demonstrated that nickel NHC complexes are more active in oxidative addition reactions than palladium.[31] Nickel has been shown to have catalytic properties in a range of reactions, including the activation of the C–F

bond, which is a challenging task for researchers.[32,33] Nickel-catalyzed transformations often employ high temperatures, as reductive elimination is the rate-limiting step. Ligands with electron acceptor substituents are designed to facilitate this stage, making nickel a cost-effective alternative to palladium.

There are only a few examples of Ni/NHC complexes with electron acceptor substituents in the aromatic rings in the literature, and their properties and applicability have not been well explored to date. For example, the combination of nickelocene and 1,3-bis(2,6-dimethyl-4-bromophenyl)imidazol-2-ylidene produces a carbene complex through a one-step synthetic route. The structure of the complex was studied using X-ray diffraction, which revealed the presence of bromine in the NHC structure. The coordination of the carbene in the complex results in structural changes, including torsion of the aryl rings to minimize steric interactions with the η^5-Cp ligand.[34] The electrochemical properties of the IMes-coordinated complexes were compared to those of the F-substituted NHC ligand complexes in this study. The IMes-coordinated complexes exhibited initial oxidation events that were well separated from a second oxidation process in the cyclic voltammograms. Similarly, the cyclic voltammograms of the complexes containing F-substituted NHC ligands also revealed two separate oxidation waves. The absolute potentials as well as the separation between the two waves varied with the substitution pattern, suggesting that the NHC ligand environment is an interesting platform for the development of new redox-triggered reactions that release trifluoromethyl and perfluoroalkyl radicals upon oxidation.[35]

[a]Zelinsky Institute of Organic Chemistry, Russian Academy of Sciences, Leninsky prospekt 47, Moscow, 119991, Russia. E-mail: val@ioc.ac.ru; https://AnanikovLab.ru

[b]Department of Chemistry, Lomonosov Moscow State University, Leninskii Gory 1-3, Moscow 119991, Russia

[c]Kurnakov Institute of General and Inorganic Chemistry, Russian Academy of Sciences, Leninskii pr. 31, Moscow 119991, Russia

Fluorine is the most appropriate substitute for investigating the electronic characteristics of ligands, as it has the least steric hindrance on the ligand out of all available substituents. The additional interest in the role of fluorine in the study of inorganic and organometallic molecules stems from its potential biological activity[36] and its possible involvement in intermolecular interactions that may accelerate catalytic processes.[37,38] In particular, CF–π interactions can affect the conformation and geometry of the catalyst and stabilize specific conformations of molecules, which are essential for catalytic activity.[39] Therefore, studying the effect of acceptor substituents, especially fluorine, on catalyst properties is an important task for researchers.

In our present study, we embarked upon the synthesis of Pd/NHC$_F$ and Ni/NHC$_F$ complexes featuring fluorine atoms positioned at various locations within the aromatic ring. Our objective extended beyond mere synthesis; we aimed to investigate the impact of the position and number of fluorine atoms within the NHC ligand framework on its electronic characteristics and, consequently, its catalytic efficacy (Fig. 1). This systematic exploration involved comprehensive analyses employing both structural and spectroscopic studies, thereby delving into the nuanced intricacies of molecular structure and reactivity.

Results and discussion

We chose 4-fluoro- **1b**, 2,4-difluoro- **1c**, 3,4-difluoro- **1d**, 2,6-difluoro- **1e**, 3,5-difluoro- **1f**, 2,3,4-trifluoro- **1g**, 2-fluoro- **1h**, 3-fluoro- **1i** and 2,4,6-trifluoro- **1j** substituted anilines, to investigate the effect of substituent position on the properties of the NHC ligands, as well as the unsubstituted aniline **1a**, for comparison. NHC$_F$ salts **2a–g** and **2j** were prepared in a one-pot manner without the isolation of the intermediate diazadiene, and the remaining fluorine-substituted salts were successfully separated by extraction from water (Fig. 2). The imidazolium salt **2f** was isolated in 13% yield. Compounds **2h** and **2i** were synthesized as previously described under very mild conditions.[40] The resulting products were suitable for the synthesis of Pd/NHC$_F$ complexes without prior purification; however, additional purification was performed using a chromatographic column with an eluent (DCM/MeOH 13 : 1) to obtain Ni/NHC$_F$, because Ni/NHC$_F$ complexes cannot be purified on a chromatographic column without decomposition. The resulting imidazolium salts, except for **2e**, exhibit intense blue fluorescence under ultraviolet light when analyzed by thin-layer chromatography, making isolation easier. The challenge in the synthesis of imidazolium salts is connected with the substitution patterns of their aryl rings. Substitution in the *o*- or *p*-positions, or only in the *p*-position, gives the highest yields. If the *p*-position is unsubstituted, the yield of the final imidazolium salt is significantly reduced. If all three positions are unsubstituted, additional side reactions occur, further reducing the overall yield. This phenomenon cannot be attributed to the low nucleophilicity of fluoroanilines since, as a result of the reaction, no initial aniline remains, but a large number of byproducts and resins are formed.

(NHC$_F$)PdCl$_2$Py complexes were prepared using a previously described method, with a slight decrease in yield for complexes **3e**, **3f** and **3j** (Table 1).[40,41] Complexes **3a–j** are air- and moisture-stable compounds that are almost insoluble in water and nonpolar organic solvents. The synthesis of compound **3ja** {1,3-bis[2,4,6-trifluorophenyl]-imidazol-2-ylidene}dichloro(pyridine) palladium, carried out under the same conditions as the other complexes, yielded the product **3jb** (SP-4-1)-[[2,2′-(1*H*-Imidazole-1,3(2*H*)-diyl-κC^2)bis[4,6-bisfluorophenolato-κO]](4-)] (pyridine)palladium containing chelated O-groups in the *o*-position instead of fluorine atoms. The resulting complexes were successfully separated by column chromatography. The structures of the complexes were confirmed by NMR, MS and X-ray diffraction. (NHC$_F$)Ni(Cp)Cl complexes **4a–j** were obtained in yields of 11–86% by nickelation of the NHC$_F$ proligands **2a–j** using NiCp$_2$ in dry DMF. Comparing the reaction mass after the reaction with the isolated yield, it can be concluded that some of the obtained Ni/NHC$_F$ complexes are extremely sensitive to trace amounts of water, which greatly complicates their isolation (including decomposition on silica gel and alumogel) and significantly reduces the overall yield of the reaction. The Ni/NHC$_F$ complexes purified exclusively by recrystallization have been fully characterized by various techniques (see Experimental section and ESI†).

Herein, we report the crystal structures of **4b**, **4c**, **4d**, **4e**, **4g**, **4h** and **3jb** (Fig. 3). To our surprise, the structures of nickel complexes with electron-withdrawing substituents have previously been poorly represented.[42] In all the determined structures, the Cp ring is symmetrically coordinated to Ni^{2+}, and ring slippage is not observed. The Ni^{2+} cation (C.N. = 5) is located in a pseudotrigonal environment: the Ni, Cl and C1 atoms and the Cp(centroid) are located in the same plane, and the sum of the three angles about the Ni atom is 360° (Table S11†). Selected geometrical parameters for the Cp–Ni (Cl)–C crystallographic node are provided in Tables 2 and S11.† When comparing the geometric parameters of compounds **4c** and **4g**, it can be observed that the presence of a fluorine atom in the *m*-position slightly increases the bond length of Ni–C1 (from 1.863(1) to 1.874(1)). Similarly, a comparison of compounds **4d**, **4g** and **4h** revealed that the intro-
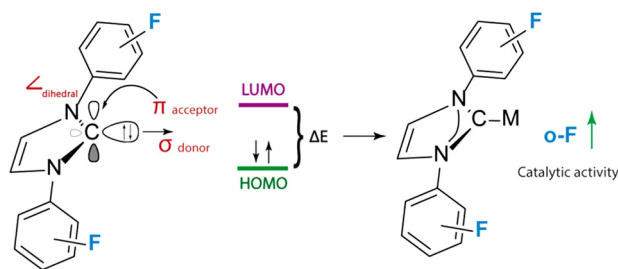
Fig. 1 Analysis of the influence of the number of fluorine atoms and their position on the individual electronic and steric parameters of the NHC$_F$ ligands and M\NHC$_F$ complexes.
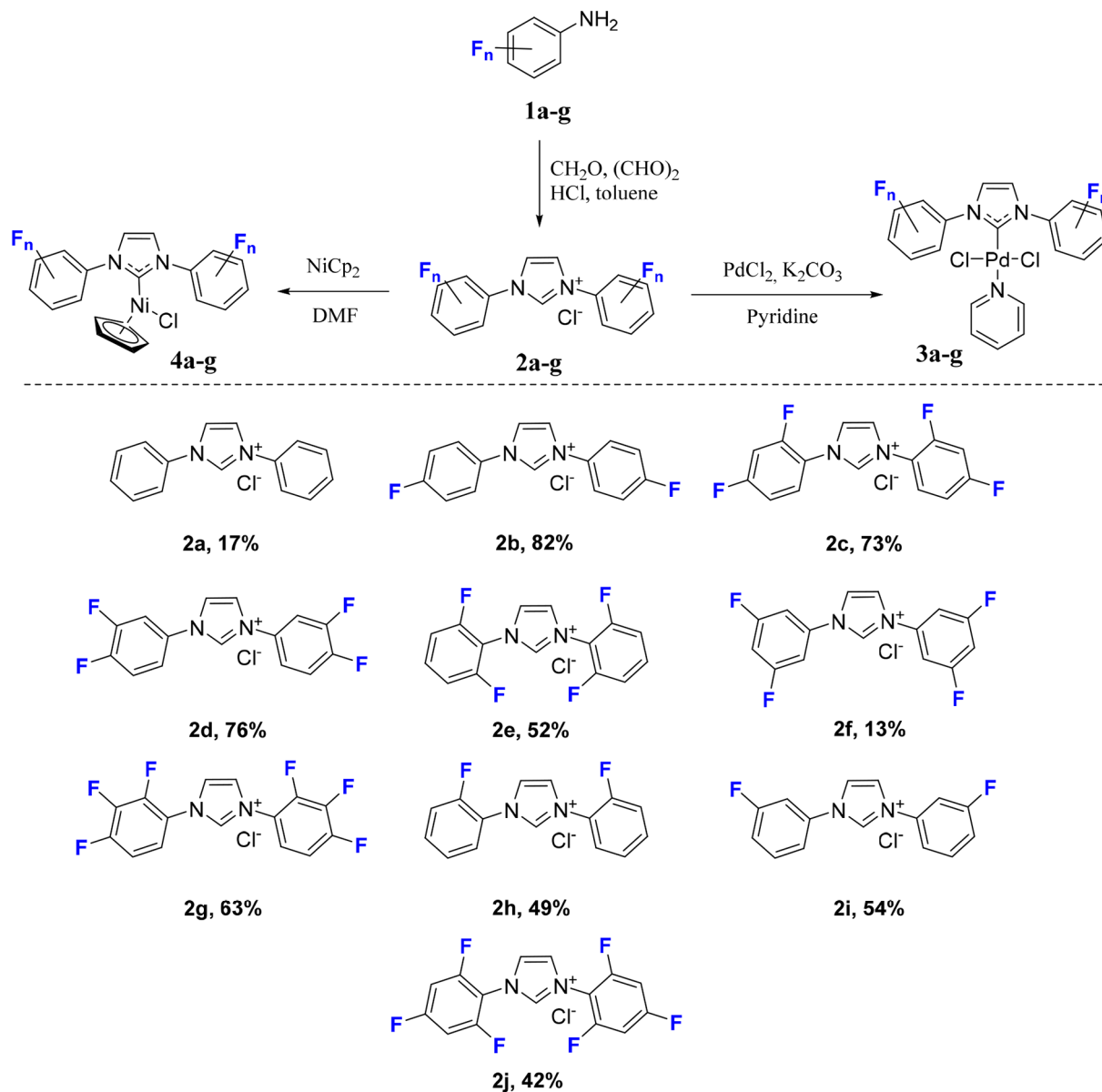
Fig. 2 Common scheme of the synthesis of compounds and the preparation of NHC$_F$ salts **2a–j**, complexes of Pd/NHC$_F$ **3a–j** and Ni/NHC$_F$ **4a–j**.

Table 1 Yields of synthesized complexes **3a–j** and **4a–j**

	Yield, %									
	H	4-F	2,4-F	3,4-F	2,6-F	3,5-F	2,3,4-F	2-F	3-F	2,4,6-F
Complex	**a**	**b**	**c**	**d**	**e**	**f**	**g**	**h**	**i**	**j**
Pd/NHC$_F$ **3**	66	56	54	63	39	45	58	62	71	37[a]
Ni/NHC$_F$ **4**	46	73	64	75	35	28	86	11	24	46

[a] The yield is equal to the sum of the individual outputs of the two substances **3ja** (31%) and **3jb** (6%).

duction of an *o*-substituent results in a shortening effect. According to the X-ray crystallographic data, a correlation was observed between the Ni–NHC bond length and the dihedral angles between the phenyl and imidazolium rings. By comparing complexes **4b** and **4d**, we can argue that the presence of fluorine in the *meta*-position, in combination with a *p*-substituent, has a negligible effect on the length of the Ni–C1 bond but increases the dihedral angle of the complex. Notably, in
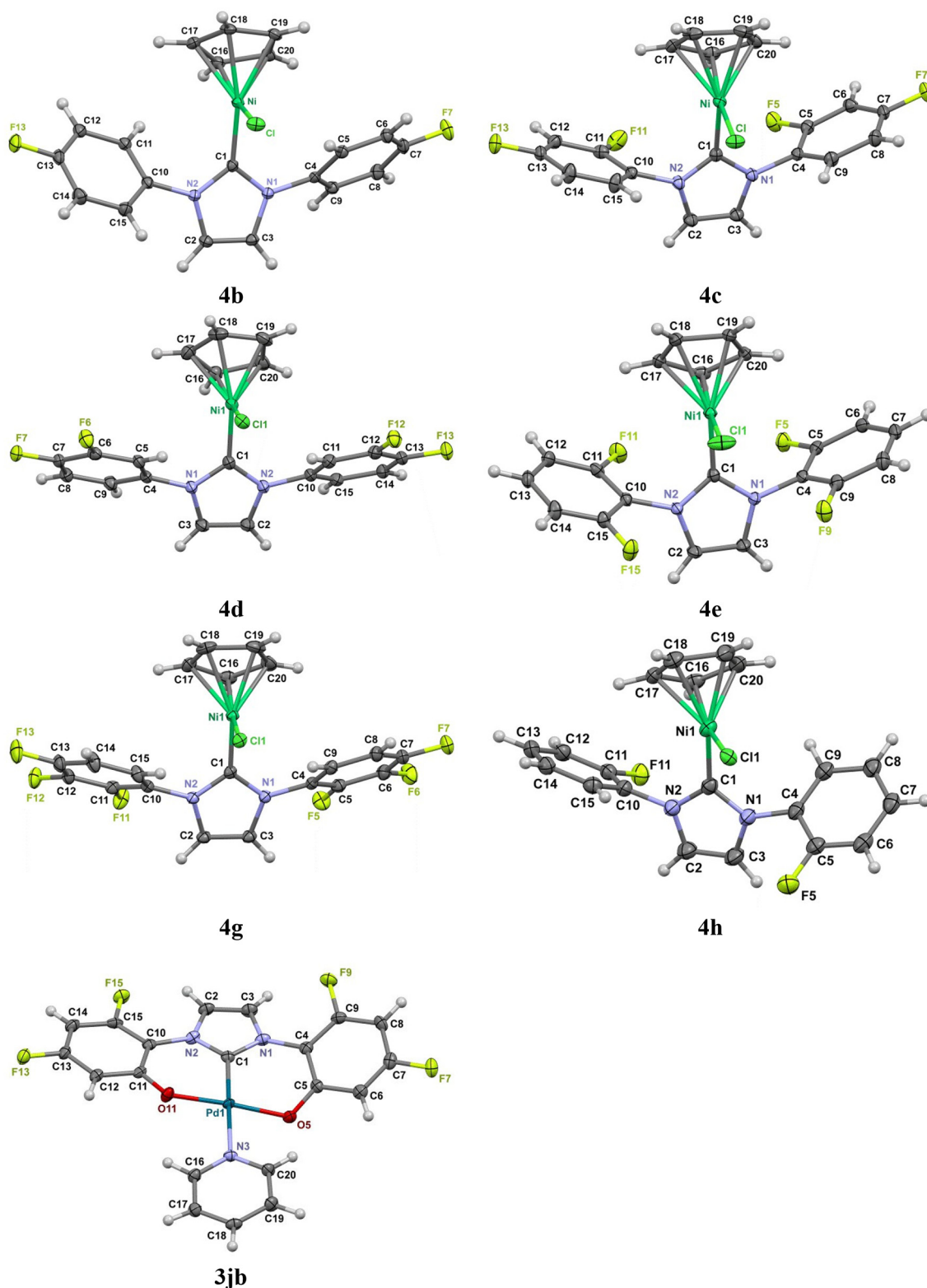
Fig. 3 Crystal structures of complexes **4b–4e**, **4g–h**, **3jb**, and ORTEP diagrams (disorders for **4c–4e** and **4g** are omitted; thermal ellipsoids are set to a 50% probability level).

complexes **4c** and **4e**, the dihedral angles are quite similar, although complex **4c** contains a *p*-fluoro substituent and complex **4e** contains two *o*-substituents. In the **4h** complex

containing one fluorine at the *o*-position, the dihedral angle is smaller. Considering the dihedral angles in the **4g** and **4c** structures, it can be observed that the dihedral angles in **4g**

Table 2 Selected geometrical parameters for the Cp−Ni(Cl)−C crystallographic node (Å, °) for **4**

	4b	4c	4d	4e	4g	4h
Bond Ni–C1	1.888(1)	1.863(1)	1.883(2)	1.864(1)	1.874(1)	1.863(1)
Bond Ni–Cl1	2.1905(4)	2.1953(4)	2.2154(4)	2.1860(4)	2.2059(4)	2.1953(4)
Distance Cp(centroid)⋯Ni	1.7647(7)	1.761(2)	1.757(2)	1.774(1)	1.751(1)	1.7688(8)
Angle N_2C_3/Ph (C4⋯C9)	49.91(4)	80.13(5)	40.79(6)	88.01(4)	45.38(6)	61.62(7)
Angle N_2C_3/Ph (C10⋯C15)	53.14(6)	78.55(5)	42.92(6)	77.68(5)	49.47(5)	67.11(6)
Angle Cp(centroid)–Ni1–Cl1	128.7	133.8	131.4	134.1	130.6	127.3
Angle Cp(centroid)–Ni1–C1	136.6	131.8	127.9	132.7	131.2	132.9

are smaller than those in **4c**. The dihedral angle decreased during the transition from **4g** to **4d**, in the absence of the *o*-fluorine atom. This indicates that the *o*-substituent increases the dihedral angle, which explains why **4e** has the highest dihedral angle value in the given series of crystals. Despite the fact that fluorine has a small atomic radius, it has a steric effect, both in crystals and in solutions. This was observed in our previous studies, where we investigated the steric effect of a *o*-substituent on M/NHC complexes, and the dependence of σ- and π-bonds stabilization energy on the dihedral angle between the phenyl and imidazolium rings.[40,41,43] Huynh and coworkers have also previously discovered the importance of the dihedral angle in modulating the electronic properties of NHCs, especially with respect to their σ- and π-bonds. When the dihedral angle between the wingtip substituent and the carbene plane changes, it affects the energies of the HOMO and π-HOMO orbitals. As the phenyl ring changes its orientation from coplanar ($\theta = 0°$) to perpendicular ($\theta = 90°$), the HOMO becomes slightly destabilized. Conversely, the π-HOMO energy significantly increases as the two planes align ($\theta = 90 \rightarrow 0°$).[44] The stabilization energy for both the σ- and π-bonds reached a maximum at a dihedral angle of 90 degrees and a minimum at an angle of 0 degrees. Applying these findings to our current data, we can assert that a complex with two *o*-substituents has the shortest Ni–C1 bond because the strong σ-bond in this complex is stabilized by the *o*-substituents, and the dihedral angle is close to 90 degrees, which maximizes the stabilization energy. Palladium complex **3jb** was obtained and fully characterized. Further information on the geometry of the complex in its crystal structure can be found in the ESI.†

To assess the impact of fluorine substitution on the σ- and π-contributions to the M−NHC bond, a series of experiments was conducted. We first measured the chemical shifts in the ^{13}C NMR spectra of the C2 carbon atom in imidazolium salts **2a–j** and then arranged the ligands and complexes in order of decreasing σ-donor strength (Table 3). Note that the ranking of NHC donor capacity by the ^{13}C NMR signal of the carbene atom of the NHC itself is applicable only to NHCs of the same type in similar complexes. Additionally, one of the tools available for evaluating the σ-donor abilities of NHC ligands is the one-bond CH *J*-coupling value ($^{1}J_{CH}$ in NHC salts), which is related to the hybridization of the carbon atom involved.[45] Higher $^{1}J_{CH}$ constants correspond to poorer σ-donating properties of NHC ligands due to the increased s-orbital character of the C–H bond.[46] The one-bond CH *J*-coupling constants

obtained from the ^{1}H-coupled ^{13}C NMR spectra showed good correlation with the ^{13}C shifts in the C2 carbon data. The ^{13}C NMR chemical shift data of the C2 carbon in the Pd/NHC$_F$ complexes also agree well with these values. Analysis of the data shows that the one-bond CH *J*-coupling constant changes from 225.4 Hz for **2a** to 230.5 Hz for **2e**, indicating that the introduction of fluorine at any position on the phenyl ring decreases the σ-donor properties of the ligand. The strongest σ-donors in the series are nonfluorinated salt **2a** and *p*-fluorinated salt **2b**. To assess the donation properties of obtained ligands, we compared their properties with literature data. We found that the J_{CH} value for compounds **2e**, **2h** and **2j** is higher than for most known imidazolium ligands, including 4,5-Cl$_2$-substituted (229.0).[47] On average, the constant value is lower for compounds that don't contain acceptor substituents.[48,49]

To investigate the influence of the fluorine position in the substituent on the π-contribution to the M/NHC bond, a series of selenones **5a–j** were synthesized by reacting an imidazolium salt with elemental selenium in the presence of triethylamine in DMF under air conditions.[50] NMR spectra of ^{77}Se were recorded to determine the chemical shift of ^{77}Se, which correlates with the π-acceptor properties of the ligand.[51,52] The order of increase in π-acceptance was **5f** > **5g** > **5d** > **5j** > **5i** > **5c** ≈ **5e** > **5h** > **5b** > **5a** (Fig. 4, see ESI†).

Based on the analysis of the data in Table 3, it can be concluded that the decrease in σ-donation occurred almost linearly in the selected series, and the effect of the substituent varied depending on the position of the substituent (Table 3A). The greatest influence on the increase in the ^{13}C chemical shift is exerted by *o*-substituents, which is confirmed by the increase in the chemical shift for all compounds containing the *o*-fluorine substituent **2c**, **2e**, **2g**, **2h** and **2j**. It can be concluded that the reduction in the σ-donor properties of the ligands is most influenced by the presence of acceptor substituents at the *o*-positions (on average, approximately 3.5 ppm per fluorine atom), followed by substituents at the *m*- and *p*-positions with approximately the same magnitude. Notably, the substituents at the *o*-positions completely canceled out the overall effect on the chemical shift, whereas those at the *meta*-positions, in contrast, enhanced it. In particular, the increase in the ^{13}C chemical shift and the spin–spin interaction constant J_{CH} are almost linear. By estimating the change in the J_{CH} constant compared to the change in chemical shift, we would expect a straight line. However, we observe distinct peaks for **2e** and **2g**, and a local minimum for the **2i** and **2h** ligands,

Table 3 Dependence of the electronic parameters of the NHC$_F$ ligand on the increase in the ^{13}C chemical shift. (A) Plot of J_{CH} *vs.* ^{13}C (C2) for NHC$_F$ salt **2**. (B) Plot of the chemical shift of ^{77}Se for selenones **5** *vs.* ^{13}C (C2) for NHC$_F$ salt **2**. (C) Plot of the %V_{bur} *vs.* ^{13}C (C2) for NHC$_F$ salt **2**. %V_{bur} is calculated for complexes **3**
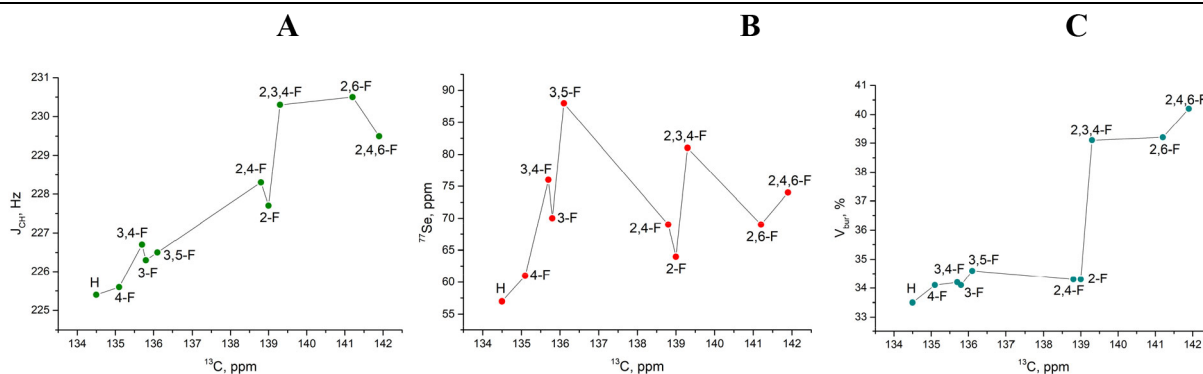
	^{13}C(C2), ppm (**2**)	^{13}C(C2), ppm (**3**)	^{13}C(C2), ppm (**4**)	^{77}Se, ppm (**5**)	J_{CH}, Hz (**2**)	%V_{bur} (**3**)
H **a**	134.5	151.4	166.1	57	225.4	33.5
4-F **b**	135.1	152.6	166.8	61	225.6	34.1
3,4-F **d**	135.7	154.1	168.5	76	226.7	34.2
3-F **i**	135.8	153.1	167.7	70	226.3	34.1
3,5-F **f**	136.1	154.9	169.8	88	226.5	34.6
2,4-F **c**	138.8	156.2	170.6	69	228.3	34.3
2-F **h**	139.0	155.0	169.5	64	227.7	34.3
2,3,4-F **g**	139.3	157.6	172.4	81	230.3	39.1
2,6-F **e**	141.2	160.3	175.4	69	230.5	39.2
2,4,6-F **j**	141.4	152.0^a	176.7	74	229.5	40.2

^{a} Chemical shift is given for the **3ja** complex.
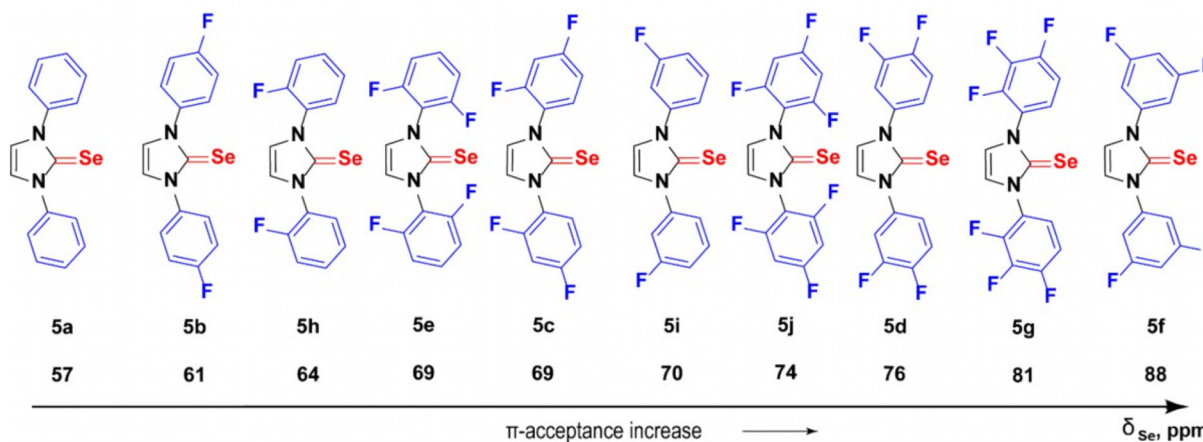
Fig. 4 Estimation of the π-acceptance abilities of NHC ligands by NMR ^{77}Se chemical shifts in CDCl₃.

indicating that the decrease in donation as assessed by the J_{CH} may be greater than that predicted by chemical shift analysis. The ^{77}Se chemical shifts of selenone derivatives **5a–j** were also evaluated in a series with decreasing σ-donor properties. Notably, for **5f** and **5i**, there was a significant increase in π-acceptance with a relatively minor decrease in σ-donation. Increased π-acceptance was also observed for **5d** and **5g** (Table 3B). Since palladium complexes **3** showed little or no cata-

lytic activity, they are useful for studying the effects of substituents on their properties (see ESI†). The %V_{bur} parameter was evaluated only for palladium complexes **3**. The evaluation of the influence of acceptor groups on the increase in %V_{bur} shows a sharp increase in three cases – when a fluorine atom is introduced in the *m*-position in 2,4-difluoro-(2,3,4-trifluoro-) compounds and in the presence of two *o*-fluorine substituents in compounds 2,6-difluoro- and 2,4,6-trifluorosubstituted (Table 3C).

Based on the data presented in a previously published study, the introduction of fluorine reduces the energy levels of the HOMO and LUMO.[40] In particular, the introduction of a fluorine atom into the *m*-position of the phenyl ring lowers the energy of these orbitals more than that of the *o*- and *p*-substituents do, while the energy gap (E_{0-0}) between them remains relatively unchanged. To determine these changes in fluoro-, difluoro- and trifluoro-substituted Ni/NHC$_F$ complexes, we used photoluminescence methods.

Fig. 5 presents the absorption and normalized photoluminescence spectra of Ni/NHC$_F$ complexes **4a–4j** in dichloromethane. The resultant compounds exhibit absorption within the range of 225–375 nm, with a molar extinction coefficient of 10^3 M^{-1} cm^{-1}. These absorption features can be attributed to both ligand–metal and ligand-to-ligand charge transfer transitions.[53] Absorption in the wavelength range of 450–550 nm is associated with electronic transitions in the Cp–Ni–Cl system. As seen from the absorption data, with the addition of fluorine substituents, the absorption peak at 505 nm shifted slightly to shorter wavelengths. This shift corresponds to an increase in the energy gap between the HOMO and LUMO, which is a con-

sequence of a reduction in electron density within the Cp–Ni–Cl system.

The photoluminescence spectra of the complexes, when irradiated with UV (λ_{exc} = 260 nm), exhibit a characteristic peak with a narrow emission band. The characteristics of this emission line are presented in Table 4. When fluorine is introduced into the molecule, an increase in the intensity of luminescence is observed for compounds **4c–4d**, **4g**, and **4j**, which generally improves the luminescent characteristics of the complexes. When fluorine is introduced at only one *o*- or *m*-position, the highest luminescence intensity is observed for the complexes. At the same time, correlations were observed in the presence of fluorine at the *o*-position; the luminescence intensity of the complex was significantly greater than that of complexes without fluorine at this position. Additionally, upon the addition of fluorine to the molecule, the primary peak shifts toward shorter wavelengths. In the case of compounds **4b** and **4f**, in particular, a shift toward longer wavelengths was observed. It is worth mentioning that the luminescence intensities of these compounds were lower than those of their analogs. However, for compound **4g**, which has *o*-, *m*- and
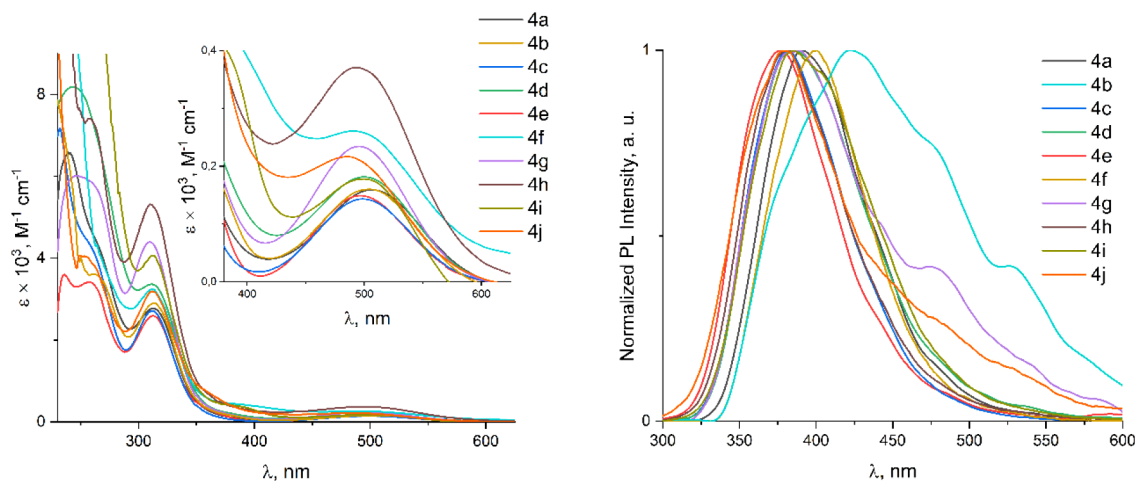

Fig. 5 Absorption spectra of Ni/NHC$_F$ **4** in dichloromethane (left). Normalized photoluminescence spectra of the complexes in dichloromethane at λ_{exc} = 260 nm (right).

Table 4 Electrochemical, optical data and calculated frontier orbital energy values of Ni/NHC$_F$ complexes **4**

Compound	λ_{max}, M^{-1} cm^{-1}	E_{0-0}, (eV)	E_{HOMO}, eV	E_{LUMO}, eV	Gap, eV	λ_{em}, nm	FWHM λ_{em}, nm
H **4a**	505	2.01	−4.86	−3.27	1.59	390	40
4-F **4b**	488	2.02	−4.77	−3.25	1.52	419; 486	40; 68
2,6-F **4e**	498	2.13	−4.95	−3.37	1.58	381	38
2,4-F **4c**	499	2.14	−4.81	−3.27	1.54	377	38
3,4-F **4d**	496	2.11	−4.89	−3.11	1.78	385	43
3,5-F **4f**	500	2.12	nd	nd	nd	403	37
2,3,4-F **4g**	492	2.14	−4.89	−3.66	1.29	380; 474	31; 64
2-F **4h**	493	2.10	nd	nd	nd	388	40
3-F **4i**	498	2.17	nd	nd	nd	370; 404	23; 35
2,4,6-F **4j**	485	2.14	nd	nd	nd	371; 406; 470	30; 40; 68

Conditions: the voltammograms were recorded in 0.1 M Bu$_4$PF$_6$/MeCN electrolyte (water content <20 ppm/0.5 mM) on a glassy carbon disc electrode at a scan rate of 100 mV s^{-1}. The concentration of the analytes was 2.5 mM in all cases.

p-fluoro-substituents, a sharp decrease in the luminescence intensity and the appearance of an additional peak at 474 nm were observed.

The energy levels of the HOMO and LUMO were calculated based on the electrochemical data using previously proposed formulas:

$$E_{\text{LUMO}} = -(E_{[\text{semidif,red } vs. \text{ Fc+/Fc}]} + 4.8)(\text{eV});$$
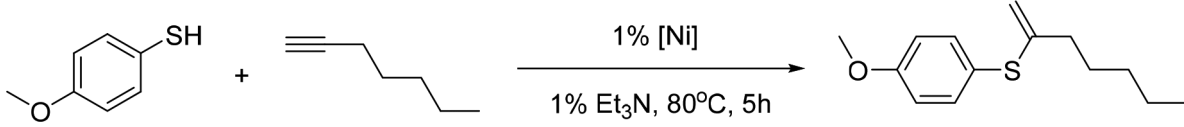
$$E_{\text{HOMO}} = -(E_{[\text{semidif,red } vs. \text{ Fc+/Fc}]} + 4.8) \ (\text{eV}).[54]$$

During the exploration of nickel complex **4**, which contained ligands with varying numbers of fluorine atoms, a clear trend in electrochemical properties was observed (refer to Table 4). The **4h**–**4j** complexes decompose rapidly in solution, so measurements could not be made for them. As the fluorine content increased, there was a noticeable shift in the oxidative potential, resulting in a decrease in the energy of the HOMO. This shift is indicative of the strong electron-withdrawing effect of fluorine, which stabilizes the HOMO and lowers its energy level. The presence of fluorine atoms in the *o*-, *m*-, and *p*-positions of complex **4g**, within the phenyl fragment significantly reduced the energy gap. This indicates that the spatial configuration of the electronegative fluorine atoms is important for modulating the electronic structure of the complexes. Furthermore, when fluorine is located solely in the *m*- and *p*-positions of the phenyl group in the imidazolium ion, there is a significant increase in the energy of the HOMO. This finding suggested that the interaction between fluorine atoms and the diazole ring can result in different electronic effects, depending on their position. The observed differences can be explained by the influence of fluorine substitution on the aromatic positions, which alters the conjugation and electronic distribution within the ligand system. This, in turn, affects the energy of the molecular orbitals.

In order to assess the impact of introducing fluorine atoms into various positions of the phenyl ring in NHC, in comparison to the unsubstituted complex, the catalytic activity of the complexes was evaluated in the synthesis of vinyl sulfides, involving the addition of the S–H bond from thiols to alkynes (Table 5). This reaction has been studied in the case of Ni (acac)$_2$, and a variety of different addition products can form.[55] During this reaction in the presence of M/NHC complexes with donor ligands, only one product was formed.[56] In this work, Markovnikov-type addition leading to β-vinyl sulfide was achieved under conditions catalyzed by Ni/NHC$_F$ **4** complexes with high selectivity. The optimal reaction time was determined to be 5 hours, as an increase in the reaction time to 48 hours resulted in the polymerization of the alkyne. It can be reasonably assumed that this was due to the degradation of the nickel complexes after an average of 5 hours of reaction.

The results of catalytic studies on Ni/NHC$_F$ complexes **4a–j** have shown that the incorporation of a fluorine atom at the *p*-position can both increase the yield of the reaction, as in the case of **4h**, compared to **4c** and **4i** compared to **4d**, and lower it, as in the case of **4e** and **4j** (Table 5). Similarly, the incorporation of fluorine at the *m*-position, as in **4d**, increases the yield of vinyl sulfide formation compared to that of **4b**, but **4g** has a lower yield compared to **4c**. Complexes with two substituents, one of which is *o*-F (**4c**, **4e**), increase the reaction yield, whereas complexes with three substituents (**4g**, **4j**) decrease it. The presence of an *m*-F substituent on the phenyl ring in the compound **4i** decreased the reaction yield compared to that of unsubstituted complex **4a**, whereas the presence of two substituents at both *m*-positions in compound **4f** increased the yield, although this increase was not significant. A similar effect, however, is more pronounced when *o*-substituents are introduced into one or two positions of the phenyl ring in compounds **4h** and **4e**. The maximum yield was obtained with compound **4e**, which has two substituents at the *o*-positions.

Table 5 Catalytic activities of Ni/NHC$_F$ complexes **4** as a precatalyst in the addition of ArSH to heptyne[a,b]


Entry	[Ni]	Substituent	Yield,[a] %
1	—	No cat	0
2	**4a**	H	44
3	**4b**	4-F	41
4	**4c**	2,4-F	53
5	**4d**	3,4-F	43
6	**4e**	2,6-F	60
7	**4f**	3,5-F	48
8	**4g**	2,3,4-F	35
9	**4h**	2-F	15
10	**4i**	3-F	26
11	**4j**	2,4,6-F	36

[a] Determined by ^{1}H NMR. [b] Reaction conditions: alkyne (2.0 mmol, in 3 portions); ArSH (2.0 mmol); [Ni] **4** (1 mol%); Et$_3$N (1 mol%); T = 80 °C; t = 5 h. The yield is equal to the conversion rate.

X-ray diffraction analysis revealed that compound **4e** has the largest dihedral angle between the phenyl imidazolium rings in the obtained series of Ni/NHC$_F$ complexes. This may be the reason why it exhibits higher catalytic activity, as it is associated with increased stabilization energy for both σ- and π-bonds in the compound. Nevertheless, when assessing the catalytic activity of compound **4g**, a reduction in yield is noted despite the larger dihedral angle relative to **4d**, suggesting a
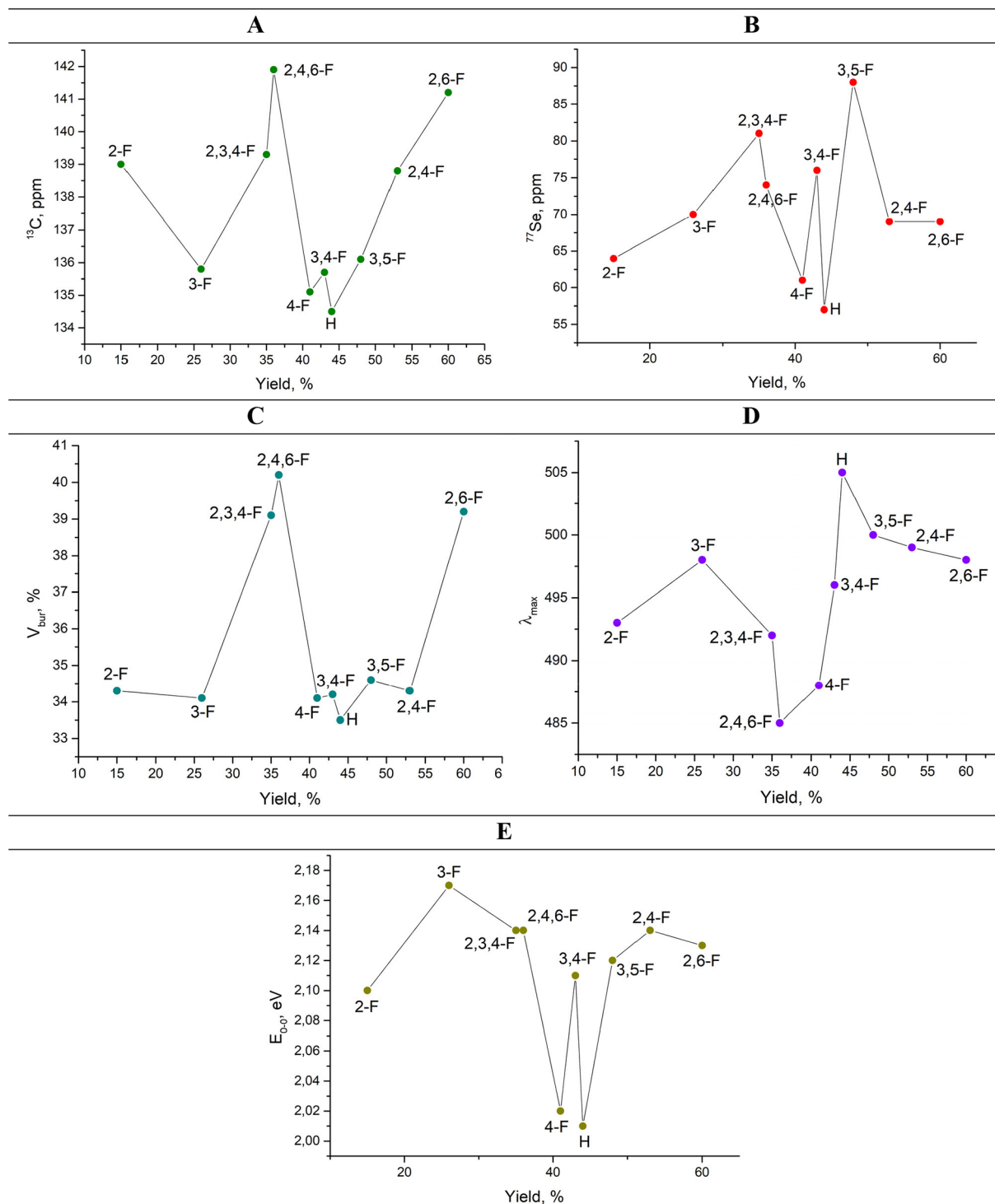
Fig. 6 Effect of the electronic parameters of the NHC$_F$ ligand on increasing the hydrothiolation yield. Plot of ^{13}C (C2) chemical shifts (A). Plot of the ^{77}Se chemical shift of selenones **5** (B). Plot of the %V_{bur} of **3a–j**. (C). Plot of the λ_{max} wavelengths of Ni/NHC$_F$ **4a–g** (D). Plot of the E_{0-0} energies of Ni/NHC$_F$ **4a–g** (E).

possible synergistic effect among the various amounts of substituents.

Based on the analysis of the changes in the σ- and π-contribution values that were previously determined, we found that both of these quantities change in a nonlinear manner as the reaction yield increases (Fig. 6). When evaluating the σ-contribution, a decrease is followed by an increase in the ^{13}C NMR chemical shift (Fig. 6A). When assessing π-acceptor properties, the chemical shifts in the ^{77}Se NMR spectra, λ_{max} wavelengths of Ni/NHC$_F$ **4a–g** and %V_{bur} did not show a clear dependence on the catalytic activity of **4a–j** (Fig. 6B–D). Nevertheless, there is a resemblance between the graphs for ^{77}Se/Yield and E_{0-0}/Yield. (Fig. 6B and E) Therefore, despite the inclusion of fluorine atoms in the study, to mitigate steric effects, it is still possible to predict some electronic properties. However, in an actual catalytic reaction, a combination of various factors influence the catalytic activity of the M/NHC complex. Identification of these factors remains an ongoing process.

Conclusions

To investigate the influence of various positions and number of substituents in the aryl ring on the characteristics of NHC compounds, synthetic pathways to prepare imidazolium salts with fluorine substituents, along with their corresponding Pd/NHC$_F$ and Ni/NHC$_F$ complexes, were proposed. A series of new Pd/NHC$_F$ and Ni/NHC$_F$ complexes were synthesized, and their structures were analyzed using experimental methods.

Incorporating acceptor substituents into the phenyl rings of NHC ligands has a significant and diverse effect on their electronic properties. Among the positions, the *o*-substituents exert the most significant influence on the electronic characteristics of the NHC ligand. Even with a low steric bulk, such as a fluorine atom, the dihedral angle between the phenyl and imidazolium rings increases, enhancing the stability of the σ- and π-components of the M–NHC bond. An investigation of the optical characteristics of Ni/NHC$_F$ compounds **4a**, **4c–e**, **4g–j** demonstrated that the incorporation of fluorine substituents increases photoluminescence by shifting the absorption and emission maxima toward shorter wavelengths (Fig. 6, bottom left). This phenomenon is attributed to the increase in the energy gap between the HOMO and LUMO, and substituents at the *o*-position have the most significant influence, while the presence of substituents at the *o*-, *m*- and *p*-positions at the same time causes the appearance of an additional emission maximum.

However, compared with other positions, *o*-accepting substituents have a greater impact on reducing the σ-donor strength of the ligand, as evidenced by the ^{13}C NMR chemical shifts and J_{CH} constants. Nevertheless, Ni/NHC$_F$ complexes containing *o*-substituents (except **4h**, **4g**) exhibited the highest catalytic activity in the hydrothiolation of alkynes. Furthermore, the *m*-substituents significantly enhance the π-acceptor character of the ligand with a relatively minor reduction in its σ-donor capability, indicating the potential utility of the ligand in eliminating

labile groups at the *trans*-position to the NHC ligand. Complexes containing ligands with *p*-substitution typically exhibit higher yields during synthesis compared to *p*-nonsubstituted ligands, highlighting their synthetic utility.

The investigation of Ni/NHC$_F$ complexes **4**, featuring ligands with varying fluorine content, revealed a clear correlation between fluorine substitution and the electrochemical properties. Particularly intriguing was the significant reduction in the energy gap observed with fluorine atoms positioned at the *o*-, *m*-, and *p*-positions within the phenyl fragment of complex **4g**. Furthermore, the distinct elevation in the energy of the HOMO when fluorine was positioned only in the *meta*- and *para*-positions of the phenyl fragment in diazole underscores the nuanced effects of fluorine substitution on the electronic structure, which are dependent on positional orientation. These findings could be highly beneficial for applications requiring precise control over electronic properties, such as in the development of organic photovoltaic materials where the alignment of HOMO and LUMO levels is critical for efficient charge transfer and energy conversion.

Concerning a plausible relationship between the studied parameters and the catalytic activity of the resulting complexes, it is possible that the increased catalytic activity observed for compounds containing two substituents in the *o*- and *m*-positions is achieved due to various factors, some of which may be opposed. Thus, catalyst fine-tuning involves solving various problems related to optimizing the electronic properties of ligands, controlling metal–ligand interactions, and ensuring the stability and efficiency of catalysts under reaction conditions, and all this accumulated knowledge will be used in future studies.

Experimental part

General information

Chemicals were obtained from P&M Invest, Sigma-Aldrich and Acros Organics. Imidazolium salts **2a–b**, **2h–i**, Pd/NHC complexes **3a–b**, **3h–i** were synthesized as described in the literature.[40,41] Selenium derivatives **5** were prepared as previously described in the literature.[50] The samples for the ESI-TOF-HRMS experiments were prepared in 1.8 mL glass vials with screw-top caps fitted with Teflon-lined septa (Agilent Technologies). NMR spectra were recorded by using Bruker Avance-NEO 300 or Bruker Fourier 300HD spectrometers operating at 300.1 MHz for ^{1}H, 75 MHz for ^{13}C, 57 MHz for ^{77}Se and 282.4 MHz for ^{19}F. ^{1}H and ^{13}C NMR chemical shifts are reported relative to the solvent signals as internal standards: 2.5 ppm/39.5 ppm for DMSO-d_6 and 7.26 ppm/77.16 for CDCl$_3$. ^{19}F NMR chemical shifts are reported relative to C$_6$F$_6$ (δ^{19}F = –162.9 with respect to CFCl$_3$). ^{77}Se chemical shifts are given in parts per million relative to the internal standard Ph$_2$Se$_2$ (δ^{77}Se = 463.27).

The electronic absorption spectra of the solutions were measured using a Cary 5000 UV-Vis-NIR spectrometer with a wavelength resolution of 0.05 nm in the range of 200–650 nm.

Photoluminescence spectra were obtained using a PerkinElmer LS-55 luminescence spectrometer with a spectral resolution of 0.5 nm and a spectral slit width of 10 nm in the range of 350–700 nm. All measurements were performed at room temperature using a standard quartz cuvette with a 1 cm optical path length and a single-position cuvette holder for liquid samples. All measurements were performed at room temperature.

Oxidation and reduction behavior of complexes **4** were analyzed by cyclic voltammetry using a digital potentiostat IPC-Pro-MF (Econix). The solution preparation and all measurements were made in an argon-filled glovebox with water and oxygen contents below 0.1 ppm. Before that, acetonitrile (HPLC grade, Acros) with an initial water content of <100 ppm was stored over 4 Å molecular sieves and preliminarily dried under oil-pump vacuum at 200–250 °C for 4 h. Bu_4NBF_4 (Sigma-Aldrich) was dried under oil-pump vacuum at 80 °C for 4 h. The water content in 0.1 M Bu_4PF_6/MeCN did not exceed 20 ppm as determined by Karl Fischer titration using a Mettler-Toledo Titrator C10SD. The compounds **4** dissolved in the supporting electrolyte with a concentration of 2.5 $\times 10^{-3}$ M were electrochemically tested in a standard three-electrode glass cell at a potential sweep rate of 100 mV s^{-1}. The working electrode was a glassy carbon disc electrode with a diameter of 1.7 mm. Before use, it was polished with abrasive paper and then GOI paste until the surface attained a mirror shine. The counter electrode was a Pt wire preannealed in a gas burner flame to remove oxides and other possible contaminations. The potentials of the studied processes were measured *versus* the Ag wire coated with AgCl (prepared by galvanostatic anodization in 5% HCl solution) separated from the bulk electrolyte solution by an electrolytic bridge filled with the supporting electrolyte. The reference electrode was calibrated *versus* the ferrocene–ferrocenium redox couple. Also, ferrocene was used as a standard to establish a one-electron current level under experimental conditions.

General procedure for the preparation of imidazolium salts 2c–g, j

An appropriate amount of amine (2 mmol) was placed in a 50 mL round-bottom flask and dissolved in toluene (10 mL). Then, glyoxal (40 wt% water solution, 117 μL, 1 mmol), paraformaldehyde (31.9 mg, 1.06 mmol) and HCl (concentrated aqueous solution, 89 μL, 1 mmol) were added. The reaction mixture was then stirred for 2 h at 60 C, after which the solvent was evaporated. The dry dark residue was transferred to a separating funnel by washing it with portions of water (50 mL) and DCM (25 mL), after which the target imidazolium salt was extracted in water. The water fraction was washed with DCM until the organic layer became colorless and was subsequently dried under vacuum.

1,3-Bis(2,4-difluorophenyl)-1*H***-imidazol-3-ium chloride (2c).** Yield 73%, white powder. ^{1}H NMR (300 MHz, DMSO-d_6) δ: 10.28 (s, 1H), 8.45 (s, 2H), 8.07 (td, J = 8.9, 5.7 Hz, 2H), 7.83 (ddd, J = 11.4, 8.9, 2.8 Hz, 2H), 7.50 (dddd, J = 9.3, 8.1, 2.8, 1.5 Hz, 2H). ^{13}C{^{1}H} NMR (75 MHz, DMSO-d_6) δ: 162.9 (dd, J = 251.1, 11.6 Hz), 155.2 (dd, J = 254.7, 13.5 Hz), 138.8, 128.7 (d, J

= 10.6 Hz), 123.9 (d, J = 2.6 Hz), 119.4 (dd, J = 11.6, 4.0 Hz), 113.0 (dd, J = 23.2, 3.8 Hz), 106.0 (dd, J = 27.8, 23.3 Hz). ^{19}F {^{1}H} NMR (282.4 MHz, DMSO-d_6) δ: −105.73 (d, J = 8.6 Hz), −118.80 (d, J = 8.6 Hz). ESI-(+) MS, m/z: 293.0697, calcd for $C_{15}H_9F_4N_2$ 293.0696 [M]$^+$, (Δ = 0.3 ppm).

1,3-Bis(3,4-difluorophenyl)-1*H***-imidazol-3-ium chloride (2d).** Yield 76%, pinkish powder. ^{1}H NMR (300 MHz, DMSO-d_6) δ: 10.64 (t, J = 1.7 Hz, 1H), 8.62 (d, J = 1.7 Hz, 2H), 8.38–8.27 (m, 2H), 7.96–7.80 (m, 4H). ^{13}C{^{1}H} NMR (75 MHz, DMSO-d_6) δ: 150.0 (dd, J = 249.4, 11.9 Hz), 149.5 (dd, J = 248.0, 13.3 Hz), 135.7, 131.1 (dd, J = 8.8, 3.4 Hz), 122.0, 119.4 (dd, J = 7.3, 3.8 Hz), 119.1 (d, J = 18.9 Hz), 112.6 (d, J = 22.3 Hz). ^{19}F{^{1}H} NMR (282.2 MHz, DMSO-d_6) δ: −135.01 (d, J = 22.6 Hz), −136.21 (d, J = 22.6 Hz). ESI-(+) MS, m/z: 293.0704, calcd for $C_{15}H_9F_4N_2$ 293.0696 [M]$^+$, (Δ = 2.7 ppm).

1,3-Bis(2,6-difluorophenyl)-1*H***-imidazol-3-ium chloride (2e).** Yield 52%, yellowish glass-like solid. ^{1}H NMR (300 MHz, DMSO-d_6) δ: 10.44 (s, 1H), 8.56 (d, J = 1.4 Hz, 2H), 7.98–7.72 (m, 2H), 7.59 (t, J = 8.7 Hz, 4H). ^{13}C{^{1}H} NMR (75 MHz, DMSO-d_6) δ: 155.9 (dd, J = 254.1, 2.5 Hz), 141.2, 133.6 (t, J = 10.0 Hz), 125.0, 113.2 (dd, J = 19.0, 3.5 Hz), 112.2 (t, J = 15.6 Hz). ^{19}F{^{1}H} NMR (282.4 MHz, DMSO-d_6) δ: −121.08. ESI-(+) MS, m/z: 293.0702, calcd for $C_{15}H_9F_4N_2$ 293.0696 [M]$^+$, (Δ = 2.0 ppm).

1,3-Bis(3,5-difluorophenyl)-1*H***-imidazol-3-ium chloride (2f).** Yield 13%, white powder. ^{1}H NMR (300 MHz, DMSO-d_6) δ: 10.63 (t, J = 1.7 Hz, 1H), 8.66 (d, J = 1.6 Hz, 2H), 8.06–7.80 (m, 4H), 7.65 (tt, J = 9.3, 2.3 Hz, 2H). ^{13}C{^{1}H} NMR (75 MHz, DMSO-d_6) δ: 162.7 (dd, J = 247.7, 14.5 Hz), 136.3 (t, J = 13.5 Hz), 136.1, 121.7, 106.7 (d, J = 30.6 Hz), 105.9 (t, J = 25.5 Hz). ^{19}F{^{1}H} NMR (282.4 MHz, DMSO-d_6) δ: −106.73. ESI-(+) MS, m/z: 293.0693, calcd for $C_{15}H_9F_4N_2$ 293.0696 [M]$^+$, (Δ = 1.0 ppm).

1,3-Bis(2,3,4-trifluorophenyl)-1*H***-imidazol-3-ium chloride (2g).** Yield 63%, yellowish oil. ^{1}H NMR (300 MHz, DMSO-d_6) δ: 10.41 (s, 1H), 8.48 (s, 2H), 7.95 (dddd, J = 10.1, 7.7, 5.1, 2.4 Hz, 2H), 7.76 (tdd, J = 9.8, 7.7, 2.3 Hz, 2H). ^{13}C{^{1}H} NMR (75 MHz, DMSO-d_6) δ: 151.3 (dd, J = 252.0, 9.5 Hz), 144.9 (ddd, J = 256.6, 12.3, 3.9 Hz), 139.5 (ddd, J = 251.2, 16.6, 13.6 Hz), 139.3, 123.9 (d, J = 2.7 Hz), 122.1 (dd, J = 8.8, 4.0 Hz), 120.4 (dd, J = 8.7, 3.8 Hz), 113.5 (dd, J = 19.0, 3.9 Hz). ^{19}F{^{1}H} NMR (282.4 MHz, DMSO-d_6) δ: −130.62 (dd, J = 22.0, 7.8 Hz), −141.41 (dd, J = 21.3, 7.9 Hz), −157.87 (t, J = 21.7 Hz). ESI-(+) MS, m/z: 329.0507, calcd for $C_{15}H_7F_6N_2$ 329.0508 [M]$^+$, (Δ = 0.3 ppm).

1,3-Bis(2,4,6-trifluorophenyl)-1*H***-imidazol-3-ium chloride (2j).** Yield 42%, white powder. ^{1}H NMR (300 MHz, DMSO-d_6) δ: 10.34 (s, 1H), 8.51 (s, 2H), 7.79 (t, J = 8.9 Hz, 4H). ^{13}C{^{1}H} NMR (75 MHz, DMSO-d_6) δ: 172.9 (d, J = 182.8 Hz), 163.0 (dt, J = 252.6, 15.3 Hz), 156.6 (ddd, J = 254.5, 16.6, 5.0 Hz), 141.4, 125.10, 109.60 (td, J = 15.9, 5.5 Hz), 102.38 (ddd, J = 28.2, 24.2, 4.0 Hz). ^{19}F{^{1}H} NMR (282 MHz, DMSO-d_6) δ: −102.16 (t, J = 7.5 Hz), −117.44 (d, J = 7.5 Hz). ESI-(+) MS, m/z: 329.0508, calcd for 329.0508 $C_{15}H_7F_6N_2$ [M]$^+$, (Δ = 0.0 ppm).

General procedure for the preparation of Pd/NHC complexes 3a–g, j

The general methodology and loading are similar to those published previously. The reactions were carried out according

to the Schlenk technique.[41] Under an argon atmosphere, the tube equipped with a magnetic stirring bar was loaded with imidazolium salt **2** (0.30 mmol), PdCl$_2$ (0.29 mmol), K$_2$CO$_3$ (1.50 mmol) and pyridine (2 ml). After loading, the Schlenk tube was sealed and placed in an oil bath preheated to 80 °C, and stirring was continued at this temperature for 16 h. After this period, the Schlenk tube was cooled, and the reaction mixture was diluted with DCM and passed through 1 cm of Celite. The solvents were evaporated, and the resulting mixture was purified by column chromatography (DCM/EtOAc 20 : 1, silica gel) to afford the corresponding Pd/NHC$_F$ complex **3**.

{1,3-Bis[2,4-difluorophenyl]-imidazol-2-ylidene}dichloro(pyridine) palladium (3c). Yield 54%, yellow powder. ^{1}H NMR (300 MHz, CDCl$_3$) δ: 8.63 (m, 2H), 8.54 (td, J = 8.7, 5.8 Hz, 2H), 7.68 (tt, J = 7.7, 1.7 Hz, 1H), 7.33 (d, J = 1.6 Hz, 2H), 7.26–7.20 (m, 2H), 7.19–7.02 (m, 4H). ^{13}C{^{1}H} NMR (75 MHz, CDCl$_3$) δ: 163.2 (dd, J = 252.7, 11.0 Hz), 157.2 (dd, J = 255.6, 12.6 Hz), 156.2, 151.3, 138.2, 131.3 (d, J = 10.0 Hz), 124.6, 124.4 (d, J = 2.7 Hz), 123.31 (dd, J = 11.9, 3.8 Hz), 112.1 (dd, J = 22.5, 3.9 Hz), 105.4 (dd, J = 26.7, 23.0 Hz). ^{19}F{^{1}H} NMR (282.4 MHz, CDCl$_3$) δ: −107.52 (d, J = 8.0 Hz), −118.36 (d, J = 8.0 Hz). ESI-(+) MS, m/z: 513.9765, calcd for C$_{20}$H$_{13}$ClF$_4$N$_3$Pd 513.9766 [M]$^+$, (Δ = 0.2 ppm).

{1,3-Bis[3,4-difluorophenyl]-imidazol-2-ylidene}dichloro(pyridine) palladium (3d). Yield 63%, yellow powder. ^{1}H NMR (300 MHz, CDCl$_3$) δ: 8.67–8.58 (m, 2H), 7.99 (ddd, J = 10.1, 6.9, 2.6 Hz, 2H), 7.84–7.76 (m, 2H), 7.65 (tt, J = 7.6, 1.7 Hz, 1H), 7.34 (q, J = 8.9 Hz, 2H), 7.26 (s, 2H), 7.24–7.16 (m, 2H). ^{13}C{^{1}H} NMR (75 MHz, CDCl$_3$) δ: 154.1, 151.2, 151.0 (dd, J = 251.8, 12.3 Hz), 150.3 (dd, J = 251.6, 13.4 Hz), 138.3, 135.3 (dd, J = 8.1, 3.6 Hz), 124.7, 123.8, 122.8 (dd, J = 6.8, 3.8 Hz), 118.2 (d, J = 18.8 Hz), 116.4 (d, J = 20.6 Hz). ^{19}F{^{1}H} NMR (282.4 MHz, CDCl$_3$) δ: −134.67 (d, J = 21.3 Hz), −136.56 (d, J = 21.4 Hz). ESI-(+) MS, m/z: 513.9752, calcd for C$_{20}$H$_{13}$ClF$_4$N$_3$Pd 513.9766 [M]+, (Δ = 2.7 ppm).

{1,3-Bis[2,6-difluorophenyl]-imidazol-2-ylidene}dichloro(pyridine) palladium (3e). Yield 39%, yellow powder. ^{1}H NMR (300 MHz, CDCl$_3$) δ: 8.68–8.60 (m, 2H), 7.61 (tt, J = 7.8, 1.8 Hz, 1H), 7.59–7.48 (m, 2H), 7.28 (s, 2H), 7.17 (m, 6H). ^{13}C{^{1}H} NMR (75 MHz, CDCl$_3$) δ: 160.5, 158.5 (dd, J = 256.8, 2.9 Hz), 151.5, 138.0, 131.6 (t, J = 9.6 Hz), 124.8, 124.3, 117.0 (t, J = 15.5 Hz), 112.5 (dd, J = 19.6, 3.6 Hz). ^{19}F{^{1}H} NMR (282.4 MHz, CDCl$_3$) δ: −115.79. ESI-(+) MS, m/z: 513.9762, calcd for C$_{20}$H$_{13}$ClF$_4$N$_3$Pd 513.9766 [M]+, (Δ = 0.8 ppm).

{1,3-Bis[3,5-difluorophenyl]-imidazol-2-ylidene}dichloro(pyridine) palladium (3f). Yield 43%, yellow powder. ^{1}H NMR (300 MHz, CDCl$_3$) δ: 8.74–8.68 (m, 2H), 7.87–7.74 (m, 4H), 7.72 (tt, J = 7.7, 1.6 Hz, 1H), 7.36 (s, 2H), 7.33–7.26 (m, 2H), 7.01 (tt, J = 8.6, 2.3 Hz, 2H). ^{13}C{^{1}H} NMR (75 MHz, CDCl$_3$) δ: 163.12 (dd, J = 251.0, 13.9 Hz), 155.0, 151.3, 141.0 (t, J = 12.6 Hz), 138.3, 124.8, 123.8, 110.3 (d, J = 28.7 Hz), 105.4 (t, J = 25.2 Hz). ^{19}F{^{1}H} NMR (282 MHz, CDCl$_3$) δ: −107.52. ESI-(+) MS, m/z: 473.9632, calcd for C$_{17}$H$_{11}$ClF$_4$N$_3$Pd 473.9611 [M]$^+$, (Δ = 4.4 ppm).

{1,3-Bis[2,3,4-trifluorophenyl]-imidazol-2-ylidene}dichloro(pyridine) palladium (3g). Yield 58%, yellow powder. ^{1}H NMR

(300 MHz, CDCl$_3$) δ: 8.67–8.60 (m, 2H), 8.34 (dddd, J = 9.7, 7.6, 5.1, 2.5 Hz, 2H), 7.71 (tt, J = 7.6, 1.7 Hz, 1H), 7.37 (d, J = 1.6 Hz, 2H), 7.33–7.18 (m, 4H). ^{13}C{^{1}H} NMR (75 MHz, CDCl$_3$) δ: 157.6, 152.0 (ddd, J = 254.2, 10.1, 2.6 Hz), 151.2, 147.8, 147.0 (ddd, J = 257.4, 11.8, 3.8 Hz), 140.6 (ddd, J = 254.7, 16.1, 13.7 Hz), 138.3, 124.7, 124.4 (d, J = 2.6 Hz), 124.2 (dd, J = 8.1, 4.2 Hz), 112.3 (dd, J = 18.5, 4.0 Hz). ^{19}F{^{1}H} NMR (282.4 MHz, CDCl$_3$) δ: −131.18 (dd, J = 20.7, 8.3 Hz), −141.31 (dd, J = 20.2, 8.3 Hz), −157.20 (t, J = 20.4 Hz). ESI-(+) MS, m/z: 549.9583, calcd for C$_{20}$H$_{11}$ClF$_6$N$_3$Pd 549.9578 [M]$^+$, (Δ = 0.9 ppm).

{1,3-Bis[2,4,6-trifluorophenyl]-imidazol-2-ylidene}dichloro(pyridine) palladium (3ja). Yield 31%, yellow powder. ^{1}H NMR (300 MHz, CDCl$_3$) δ: 8.66 (m, 2H), 7.65 (tt, J = 7.6, 1.6 Hz, 1H), 7.26 (s, 2H), 7.20 (m, 2H), 6.95 (m, 2H). ^{13}C{^{1}H} NMR (75 MHz, CDCl$_3$) δ: 163.2 (dt, J = 254.2, 14.2 Hz), 158.8 (ddd, J = 257.7, 15.4, 5.3 Hz), 151.4, 138.0, 129.7, 124.8, 124.3, 113.7 (d, J = 5.3 Hz), 101.4 (ddd, J = 27.2, 23.5, 4.0 Hz). ^{19}F{^{1}H} NMR (282 MHz, CDCl$_3$) δ: −104.11 (t, J = 7.1 Hz), −112.19 (d, J = 7.1 Hz). ESI-(+) MS, m/z: 588.9836, calcd for C$_{22}$H$_{14}$ClF$_6$N$_4$Pd 588.9846 [M]$^+$, (Δ = 1.7 ppm).

(SP-4-1)-[[2,2′-(1H-Imidazole-1,3(2H)-diyl-κC^2)bis[4,6-bisfluorophenolato-κO]](4-)](pyridine)palladium (3jb). Yield 6%, yellow powder. ^{1}H NMR (300 MHz, CDCl$_3$) δ: 8.88 (m, 2H), 7.99 (d, J = 1.1 Hz, 2H), 7.92 (tt, J = 7.6, 1.7 Hz, 1H), 7.54 (m, 2H), 6.62 (ddd, J = 11.0, 3.0, 1.9 Hz, 2H), 6.29 (ddd, J = 13.9, 8.4, 3.0 Hz, 2H). ^{13}C{^{1}H} NMR (75 MHz, CDCl$_3$) δ: 161.6 (dd, J = 15.1, 4.6 Hz), 160.9 (dd, J = 245.7, 18.7 Hz), 155.3 (dd, J = 246.7, 17.2 Hz), 152.0, 148.0, 138.8, 124.8, 120.5 (dd, J = 23.5, 4.9 Hz), 114.0 (dd, J = 7.0, 4.5 Hz), 103.8 (dd, J = 21.7, 2.9 Hz), 92.2 (t, J = 27.7 Hz). ^{19}F{^{1}H} NMR (282 MHz, CDCl$_3$) δ: −115.31 (d, J = 6.5 Hz), −120.86 (d, J = 6.5 Hz). ESI-(+) MS, m/z: 506.9827, calcd for C$_{20}$H$_{11}$F$_4$N$_3$O$_2$Pd 506.9825 [M]$^+$, (Δ = 0.4 ppm).

General procedure for the preparation of Ni/NHC complexes 4a–j

A 25 mL Schlenk tube equipped with a magnetic stirring bar was charged with imidazolium salt (0.5 mmol), connected to the Schlenk line and dried using the standard Schlenk procedure. In the glovebox, nickelocene (0.5 mmol) and DMF (7 mL) were added to the Schlenk tube. It was then sealed and stirred at ambient temperature for 24 h outside of the glovebox. The solvent was eventually evaporated, and the crude residue was washed with several portions of CH$_2$Cl$_2$, which was then filtered through 1 cm of Celite. The collected filtrate was concentrated to dryness to give a red powder of the desired Ni/NHC$_F$ complex **4**, which should in some cases be further purified by recrystallization in a CH$_2$Cl$_2$/hexane system. The resulting complexes were found to be quite sensitive, so column chromatography with neither silica gel nor aluminum oxide could be applied.

(IPh)Ni(Cp)Cl (4a). Yield 46%, red powder. ^{1}H NMR (300 MHz, CDCl$_3$) δ: 8.34–8.24 (m, 4H), 7.76–7.50 (m, 6H), 7.35 (s, 2H), 4.53 (s, 5H). ^{13}C{^{1}H} NMR (75 MHz, CDCl$_3$) δ: 166.1, 140.8, 129.3, 128.9, 126.3, 123.9, 92.0. ESI-(+) MS, m/z: 343.0738, calcd for C$_{20}$H$_{17}$N$_2$Ni 343.0740 [M]$^+$, (Δ = 0.6 ppm).

(4-F-NHC)Ni(Cp)Cl (4b). Yield 73%, red powder. ^{1}H NMR (300 MHz, CDCl$_3$) δ: 8.27–8.22 (m, 4H), 7.35 (t, J = 8.5 Hz, 4H), 7.32 (s, 2H), 4.58 (s, 5H). ^{13}C{^{1}H} NMR (75 MHz, CDCl$_3$) δ: 166.8, 162.7 (d, J = 249.0 Hz), 136.8 (d, J = 3.2 Hz), 128.2 (d, J = 8.7 Hz), 124.0, 116.3 (d, J = 22.9 Hz), 92.0. ^{19}F{^{1}H} NMR (282.4 MHz, CDCl$_3$) δ: −113.31. ESI-(+) MS, m/z: 414.0237, calcd for C$_{20}$H$_{15}$ClF$_2$N$_2$Ni 414.0240 [M]$^{+}$, (Δ = 0.7 ppm).

(2,4-F-NHC)Ni(Cp)Cl (4c). Yield 64%, red powder. ^{1}H NMR (300 MHz, CDCl$_3$) δ: 8.74 (td, J = 8.9, 5.8 Hz, 2H), 7.30 (d, J = 1.5 Hz, 2H), 7.25 (tdd, J = 7.7, 2.8, 1.6 Hz, 2H), 7.11 (ddd, J = 10.6, 8.2, 2.8 Hz, 2H), 4.65 (s, 5H). ^{13}C{^{1}H} NMR (75 MHz, CDCl$_3$) δ: 170.6, 163.1 (dd, J = 252.9, 10.7 Hz), 157.0 (dd, J = 253.2, 12.7 Hz), 132.6 (d, J = 10.0 Hz), 124.8 (d, J = 2.7 Hz), 124.6 (d, J = 7.3 Hz), 112.2 (dd, J = 22.4, 3.8 Hz), 104.8 (dd, J = 26.6, 23.2 Hz), 91.9. ^{19}F{^{1}H} NMR (282.4 MHz, CDCl$_3$) δ: −107.60 (d, J = 7.5 Hz), −120.45 (d, J = 7.5 Hz). ESI-(+) MS, m/z: 450.0043, calcd for C$_{20}$H$_{13}$ClF$_4$N$_2$Ni 450.0051 [M]$^{+}$, (Δ = 1.8 ppm).

(3,4-F-NHC)Ni(Cp)Cl (4d). Yield 75%, red powder. ^{1}H NMR (300 MHz, CDCl$_3$) δ: 8.20 (ddd, J = 10.6, 6.9, 2.6 Hz, 2H), 8.14–8.06 (m, 2H), 7.46 (dt, J = 9.7, 8.6 Hz, 2H), 7.34 (s, 2H), 4.65 (s, 5H). ^{13}C{^{1}H} NMR (75 MHz, CDCl$_3$) δ: 168.5, 150.8 (dd, J = 251.7, 12.7 Hz), 150.2 (dd, J = 251.1, 13.5 Hz), 136.7, 124.1, 122.8 (dd, J = 6.7, 4.2 Hz), 118.0 (d, J = 18.5 Hz), 116.2 (d, J = 20.6 Hz), 92.3. ^{19}F{^{1}H} NMR (282.4 MHz, CDCl$_3$) δ: −135.96 (d, J = 21.1 Hz), −136.99 (d, J = 21.2 Hz). ESI-(+) MS, m/z: 415.0376, calcd for C$_{20}$H$_{13}$F$_4$N$_2$Ni 415.0363 [M]$^{+}$, (Δ = 3.1 ppm).

(2,6-F-NHC)Ni(Cp)Cl (4e). Yield 35%, red powder. ^{1}H NMR (300 MHz, CDCl$_3$) δ: 7.61 (tt, J = 8.5, 6.0 Hz, 2H), 7.30–7.19 (m, 6H), 4.76 (s, 5H). ^{13}C{^{1}H} NMR (75 MHz, CDCl$_3$) δ: 175.5, 159.00 (dd, J = 255.7, 3.2 Hz), 131.6 (t, J = 9.6 Hz), 125.0, 118.3, 112.5 (dd, J = 19.5, 3.7 Hz), 92.2. ^{19}F{^{1}H} NMR (282.4 MHz, CDCl$_3$) δ: −116.76. ESI-(+) MS, m/z: 415.0346, calcd for C$_{20}$H$_{13}$F$_4$N$_2$Ni 415.0363 [M]$^{+}$, (Δ = 4.1 ppm).

(3,5-F-NHC)Ni(Cp)Cl (4f). Yield 28%, red powder. ^{1}H NMR (300 MHz, CDCl$_3$) δ: 8.01 (dd, J = 7.3, 1.7 Hz, 4H), 7.37 (s, 2H), 7.07 (t, J = 8.7, 2H), 4.71 (s, 5H). ^{13}C{^{1}H} NMR (75 MHz, CDCl$_3$) δ: δ 169.8, 163.1 (dd, J = 250.8, 13.9 Hz), 142.2 (t, J = 12.9 Hz), 124.0, 110.2 (d, J = 29.1 Hz), 104.9 (t, J = 25.0 Hz), 92.5. ^{19}F{^{1}H} NMR (282.4 MHz, CDCl$_3$) δ: −107.71. ESI-(+) MS, m/z: 415.0376, calcd for C$_{20}$H$_{13}$F$_4$N$_2$Ni 415.0363 [M]$^{+}$, (Δ = 3.1 ppm).

(2,3,4-F-NHC)Ni(Cp)Cl (4g). Yield 86%, red powder. ^{1}H NMR (300 MHz, CDCl$_3$) δ: 8.57 (tdd, J = 9.2, 5.1, 2.5 Hz, 2H), 7.43–7.27 (m, 4H), 4.69 (s, 5H). ^{13}C{^{1}H} NMR (75 MHz, CDCl$_3$) δ: 172.4, 151.8 (ddd, J = 254.5, 9.7, 2.4 Hz), 146.7 (ddd, J = 255.1, 11.9, 3.8 Hz), 140.3 (d, J = 254.2 Hz), 125.4 (dd, J = 7.8, 4.1 Hz), 125.4 (dd, J = 8.6, 3.9 Hz), 124.8 (d, J = 2.6 Hz), 112.5 (dd, J = 18.4, 4.0 Hz), 92.1. ^{19}F{^{1}H} NMR (282.4 MHz, CDCl$_3$) δ: −131.29 (dd, J = 20.7, 7.6 Hz), −143.44 (dd, J = 20.1, 7.6 Hz), −158.20 (t, J = 20.4 Hz). ESI-(+) MS, m/z: 451.0183, calcd for C$_{20}$H$_{11}$F$_6$N$_2$Ni 451.0174 [M]$^{+}$, (Δ = 2.0 ppm).

(2-F-NHC)Ni(Cp)Cl (4h). Yield 11%, red powder. ^{1}H NMR (300 MHz, CDCl$_3$) δ: 8.80 (t, J = 7.7 Hz, 2H), 7.62 (m, 2H), 7.54 (t, J = 7.6 Hz, 2H), 7.44–7.32 (m, 4H), 4.62 (s, 5H). ^{13}C{^{1}H} NMR (75 MHz, CDCl$_3$) δ: 169.5, 156.7 (d, J = 250.6 Hz), 131.4, 131.0 (d, J = 7.6 Hz), 128.2 (d, J = 11.3 Hz), 124.9 (d, J = 4.1 Hz), 124.6 (d, J = 2.3 Hz), 116.2 (d, J = 19.5 Hz), 91.8. ^{19}F{^{1}H} NMR (282 MHz, CDCl$_3$) δ: −125.37. ESI-(+) MS, m/z: 379.0552, calcd for C$_{20}$H$_{15}$F$_2$N$_2$Ni 379.0551 [M]$^{+}$, (Δ = 0.3 ppm).

(3-F-NHC)Ni(Cp)Cl (4i). Yield 26%, red powder. ^{1}H NMR (300 MHz, CDCl$_3$) δ: 8.21 (dd, J = 7.9, 1.7 Hz, 2H), 8.05 (dt, J = 9.4, 2.3 Hz, 2H), 7.65 (td, J = 8.3, 6.2 Hz, 2H), 7.36 (s, 2H), 7.35–7.27 (m, 4H), 4.62 (5, 2H). ^{13}C{^{1}H} NMR (75 MHz, CDCl$_3$) δ: 167.7, 162.6 (d, J = 248.3 Hz), 141.7 (d, J = 10.0 Hz), 130.6 (d, J = 8.7 Hz), 123.9, 122.09 (d, J = 3.3 Hz), 116.0 (d, J = 21.0 Hz), 113.8 (d, J = 25.0 Hz), 92.1. ^{19}F{^{1}H} NMR (282 MHz, CDCl$_3$) δ: −111.35. ESI-(+) MS, m/z: 379.0544, calcd for C$_{20}$H$_{15}$F$_2$N$_2$Ni 379.0551 [M]$^{+}$, (Δ = 1.8 ppm).

(2,4,6-F-NHC)Ni(Cp)Cl (4j). Yield 46%, red powder. ^{1}H NMR (300 MHz, CDCl$_3$) δ: 7.22 (s, 2H), 7.02 (t, J = 8.2 Hz, 4H), 4.79 (s, 5H). ^{13}C{^{1}H} NMR (75 MHz, CDCl$_3$) δ: 176.7, 163.3 (dt, J = 254.5, 14.3 Hz), 159.3 (ddd, J = 256.5, 15.3, 5.5 Hz), 125.2, 115.0 (td, J = 16.1, 5.2 Hz), 101.5 (ddd, J = 27.4, 23.6, 4.0 Hz), 92.2. ^{19}F{^{1}H} NMR (282 MHz, CDCl$_3$) δ: −104.11 (t, J = 7.1 Hz), −112.19 (d, J = 7.1 Hz). ESI-(+) MS, m/z: 451.0156, calcd for C$_{20}$H$_{11}$F$_6$N$_2$Ni 451.0174 [M]$^{+}$, (Δ = 4.0 ppm).

Crystallographic details. X-ray diffraction data for **4b**, **4c**, **4d**, **4e**, **4g**, **4h** and **3jb** were collected at 100 K on a Rigaku XtaLAB Synergy-S diffractometer equipped with a HyPix6000HE area-detector (kappa geometry, shutterless ω-scan technique), using monochromatized Cu K$_\alpha$-radiation. The intensity data were integrated and analytically corrected for absorption and decay by the CrysAlisPro program.[57] The structures were solved by direct methods using SHELXT[58] and refined by the full-matrix least-squares minimization method on F^2 using SHELXL-2018[59] in the OLEX2 program.[60] See the ESI for details.† The structures have been deposited at the Cambridge Crystallographic Data Center with the reference CCDC 2348102, 2338060–2338063, 2362710 and 2362711, they also contain ESI crystallographic data.†

Data availability

The data supporting this article have been included as part of the ESI.†

Conflicts of interest

There are no conflicts to declare.

Acknowledgements

References

1 A. J. Arduengo III, R. L. Harlow and M. Kline, A stable crystalline carbene, *J. Am. Chem. Soc.*, 1991, **113**, 361–363.

2 R. S. Ghadwala, Carbon-based two electron σ-donor ligands beyond classical *N*-heterocyclic carbenes, *Dalton Trans.*, 2016, **45**, 16081–16095.

3 P. Gao and M. Szostak, Hydration reactions catalyzed by transition metal–NHC (NHC = N-heterocyclic carbene) complexes, *Coord. Chem. Rev.*, 2023, **485**, 215110.

4 R. E. Andrew, L. González-Sebastián and A. B. Chaplin, NHC-based pincer ligands: carbenes with a bite, *Dalton Trans.*, 2016, **45**, 1299–1305.

5 A. Jayaraj, A. V. Raveedran, A. T. Latha, D. Priyadarshini and P. C. A. Swamy, Coordination Versatility of NHC-metal Topologies in Asymmetric Catalysis: Synthetic Insights and Recent Trends, *Coord. Chem. Rev.*, 2023, **478**, 214922.

6 G. R. P. Vasu, K. R. M. Venkata, R. R. Kakarla, K. V. S. Ranganath and T. M. Aminabhavi, Recent advances in sustainable N-heterocyclic carbene-Pd(II)-pyridine (PEPPSI) catalysts: A review, *Environ. Res.*, 2023, **225**, 115515.

7 Q. Y. Meng, L. Lezius and A. Studer, Benzylic C–H acylation by cooperative NHC and photoredox catalysis, *Nat. Commun.*, 2021, **12**, 2068.

8 E. A. Baquero, S. Tricard, Y. Coppel, J. C. Flores, B. Chaudret and E. De Jesús, Water-soluble platinum nanoparticles stabilized by sulfonated N-heterocyclic carbenes: influence of the synthetic approach, *Dalton Trans.*, 2018, **47**, 4093–4104.

9 S. Díez-González, N. Marion and S. P. Nolan, *N*-Heterocyclic Carbenes in Late Transition Metal Catalysis, *Chem. Rev.*, 2009, **109**, 3612–3676.

10 Q. Y. Meng, N. Döben and A. Studer, Cooperative NHC and Photoredox Catalysis for the Synthesis of β-Trifluoromethylated Alkyl Aryl Ketones, *Angew. Chem., Int. Ed.*, 2020, **59**, 19956–19960.

11 Z. Zuo, C. G. Daniliuc and A. Studer, Cooperative NHC/Photoredox Catalyzed Ring-Opening of Aryl Cyclopropanes to 1-Aroyloxylated-3-Acylated Alkanes, *Angew. Chem., Int. Ed.*, 2021, **60**, 25252–25257.

12 C. Wu, K. Shi, S. Li, J. Yan, Z. Feng, K. Tong, S. Zhang, Y. Zhang, D. Zhang, L. Liao, Y. Chi, G. Wei and F. Kang, Design strategies of iridium(III) complexes for highly efficient saturated blue phosphorescent OLEDs with improved lifetime, *EnergyChem*, 2024, **6**, 100120.

13 I. H. Lindenmaier, R. C. Richter and I. Fleischer, Nickel catalyzed C–S cross coupling of sterically hindered substrates enabled by flexible bidentate phosphines, *Org. Chem. Front.*, 2024, **11**, 2485–2493.

14 L. Lindh, N. W. Rosemann, I. B. Losada, S. Persson, Y. Goriya, H. Fan, O. Gordivska, K. Wärnmark, J. Uhlig, P. Chábera, A. Yartsev and P. Persson, Side-group switching between metal-to-ligand charge-transfer and metal-centered excited state properties in iron(II) N-heterocyclic carbene complexes, *Coord. Chem. Rev.*, 2024, **506**, 215709.

15 T. Zhou, G. Li, S. P. Nolan and M. Szostak, [Pd(NHC)(acac)Cl]: Well-Defined, Air-Stable, and Readily Available Precatalysts for Suzuki and Buchwald–Hartwig Cross-coupling (Transamidation) of Amides and Esters by N–C/O–C Activation, *Org. Lett.*, 2019, **21**, 3304–3309.

16 G. Li, T. Zhou, A. Poater, L. Cavallo, S. P. Nolan and M. Szostak, Buchwald–Hartwig cross-coupling of amides (transamidation) by selective N–C(O) cleavage mediated by air- and moisture-stable [Pd(NHC)(allyl)Cl] precatalysts: catalyst evaluation and mechanism, *Catal. Sci. Technol.*, 2020, **10**, 710–716.

17 L. Shen, Z. N. Chen, Q. Zheng, J. Wu, X. Xu and T. Tu, Selective Transformation of Vicinal Glycols to α-Hydroxy Acetates in Water via a Dehydrogenation and Oxidization Relay Process by a Self-Supported Single-Site Iridium Catalyst, *ACS Catal.*, 2021, **11**(21), 12833–12839.

18 M. K. Pandey and J. Choudhury, Ester Hydrogenation with Bifunctional Metal–NHC Catalysts: Recent Advances, *ACS Omega*, 2020, **5**(48), 30775–30786.

19 Z. Lu, Q. Zheng, G. Zeng, Y. Kuang, J. H. Clark and T. Tu, Highly efficient NHC-iridium-catalyzed β-methylation of alcohols with methanol at low catalyst loadings, *Sci. China: Chem.*, 2021, **64**, 1361–1366.

20 B. Maji, A. Bhandari, R. Sadhukhana and J. Choudhury, Water-soluble and reusable Ru-NHC catalyst for aqueous-phase transfer hydrogenation of quinolines with formic acid, *Dalton Trans.*, 2022, **51**, 8258–8265.

21 Z. Lu, Q. Zheng, S. Yang, C. Qian, Y. Shen and T. Tu, NHC-Iridium-Catalyzed Deoxygenative Coupling of Primary Alcohols Producing Alkanes Directly: Synergistic Hydrogenation with Sodium Formate Generated in Situ, *ACS Catal.*, 2021, **11**(17), 10796–10801.

22 T. Mandal, M. Mondal and J. Choudhury, Hypercrosslinked Polymer Platform-Anchored Single-Site Heterogeneous Pd–NHC Catalysts for Diverse C–H Functionalization, *Organometallics*, 2021, **40**(15), 2443–2449.

23 L. Kong, J. Morvan, D. Pichon, M. Jean, M. Albalat, T. Vives, S. Colombel-Rouen, M. Giorgi, V. Dorcet, T. Roisnel, C. Crévisy, D. Nuel, P. Nava, S. Humbel, N. Vanthuyne, M. Mauduit and H. Clavier, From prochiral N-heterocyclic carbenes to optically pure metal complexes: new opportunities in asymmetric catalysis, *J. Am. Chem. Soc.*, 2020, **142**, 93–98.

24 M. Micksch and T. Strassner, Palladium(II) complexes with chelating biscarbene ligands in the catalytic Suzuki–Miyaura cross-coupling reaction, *Eur. J. Inorg. Chem.*, 2012, **35**, 5872–5880.

25 T. Ritter, M. W. Day and R. H. Grubbs, Rate acceleration in olefin metathesis through a fluorine-ruthenium interaction, *J. Am. Chem. Soc.*, 2006, **128**, 11768–11769.

26 C. Xu, Y. Feng, L. R. Wang, W. P. Ma, Y. M. He and Q. H. Fan, Development of quinoline-derived chiral diaminocarbene ligands and their transition metal complexes: synthesis, structural characterization, and catalytic properties, *Organometallics*, 2020, **39**, 1945–1960.

27 M. Delgado-Rebollo, C. García-Morales, C. Maya, A. Prieto, A. M. Echavarren and P. J. Pérez, Coinage metal complexes

bearing fluorinated N-Heterocyclic carbene ligands, *J. Organomet. Chem.*, 2019, **898**, 120856.

28 Z. Wei, H. Li, Y. Wang and Q. Liu, A Tailored Versatile and Efficient NHC-Based NNC-Pincer Manganese Catalyst for Hydrogenation of Polar Unsaturated Compounds, *Angew. Chem., Int. Ed.*, 2023, **62**(23), e202301042.

29 R. Zhong, Z. Wei, W. Zhang, S. Liu and Q. Liu, A Practical and Stereoselective *In Situ* NHC-Cobalt Catalytic System for Hydrogenation of Ketones and Aldehydes, *Chem*, 2019, **5**(6), 1552–1566.

30 Z. Wei, Y. Wang, Y. Li, R. Ferraccioli and Q. Liu, Bidentate NHC-Cobalt Catalysts for the Hydrogenation of Hindered Alkenes, *Organometallics*, 2020, **39**(17), 3082–3087.

31 V. M. Chernyshev and V. P. Ananikov, Nickel and Palladium Catalysis: Stronger Demand than Ever, *ACS Catal.*, 2022, **12**, 1180–1200.

32 V. P. W. Böhm, C. W. K. Gstöttmayr, T. Weskamp and W. A. Herrmann, Catalytic C–C Bond Formation through Selective Activation of C–F Bonds, *Angew. Chem., Int. Ed.*, 2001, **40**, 3387–3389.

33 R. A. Kelly, N. M. Scott, S. Díez-González, E. D. Stevens and S. P. Nolan, Simple Synthesis of CpNi (NHC)Cl Complexes (Cp = Cyclopentadienyl; NHC = *N*-Heterocyclic Carbene), *Organometallics*, 2005, **24**, 3442–3447.

34 C. D. Abernethy, J. A. C. Clyburne, A. H. Cowley and R. A. Jones, Reactions of transition-metal metallocenes with stable carbenes, *J. Am. Chem. Soc.*, 1999, **121**, 2329–2330.

35 S. T. Shreiber, F. Amin, S. A. Schäfer, R. E. Cramer, A. Klein and D. A. Vicic, Synthesis, structure, and electrochemical properties of $[LNi(R_f)(C_4F_8)]^-$ and $[LNi(R_f)_3]^-$ complexes, *Dalton Trans.*, 2022, **51**, 5515–5523.

36 E. Rufino-Felipe, R. Colorado-Peralta, V. Reyes-Márquez, H. Valdés and D. Morales-Morales, Fluorinated-NHC Transition Metal Complexes: Leading Characters as Potential Anticancer Metallodrugs, *Anti-Cancer Agents Med. Chem.*, 2020, **21**, 938–948.

37 J. M. Serrano-Becerra, S. Hernández-Ortega, D. Morales-Morales and J. Valdés-Martínez, Bottom-up design and construction of a non-centrosymmetric network through π-π Stacking interactions, *CrystEngComm*, 2009, **11**, 226–228.

38 E. Rufino-Felipe, H. Valdés, J. M. Germán-Acacio, V. Reyes-Márquez and D. Morales-Morales, Fluorinated N-Heterocyclic carbene complexes. Applications in catalysis, *J. Organomet. Chem.*, 2020, **921**, 121364.

39 X. Xu, B. Pooi, H. Hirao and S. H. Hong, CH-π and CF-π interactions lead to structural changes of N-heterocyclic carbene palladium complexes, *Angew. Chem., Int. Ed.*, 2014, **53**, 1283–1287.

40 D. O. Prima, R. O. Pankov, A. Y. Kostyukovich, M. E. Minyaev, J. V. Burykina and V. P. Ananikov, Synthesis and characterization of Pd/NHCF complexes with fluorinated aryl groups, *Dalton Trans.*, 2022, **51**, 9843–9856.

41 R. O. Pankov, D. O. Prima, A. Y. Kostyukovich, M. E. Minyaev and V. P. Ananikov, Synthesis and a combined experimental/theoretical structural study of a com-

prehensive set of Pd/NHC complexes with o-, m-, and p-halogen- substituted aryl groups (X = F, Cl, Br, CF₃), *Dalton Trans.*, 2023, **52**, 4122–4135.

42 C. R. Groom, I. J. Bruno, M. P. Lightfoot and S. C. Ward, The Cambridge Structural Database, *Acta Crystallogr., Sect. B: Struct. Sci., Cryst. Eng. Mater.*, 2016, **72**, 171–179.

43 R. O. Pankov, D. O. Prima and V. P. Ananikov, Tailoring metal complexes with *N*-heterocyclic carbene ligands using Electron-Withdrawing Groups: Impact on catalytic activity and property development, *Coord. Chem. Rev.*, 2024, **516**, 215897.

44 V. H. Nguyen, B. M. El Ali and H. V. Huynh, Stereoelectronic Flexibility of Ammonium-Functionalized Triazole-Derived Carbenes: Palladation and Catalytic Activities in Water, *Organometallics*, 2018, **37**, 2358–2367.

45 H. A. Bent, An Appraisal of Valence-bond Structures and Hybridization in Compounds of the First-row elements, *Chem. Rev.*, 1961, **61**, 276.

46 G. Meng, L. Kakalis, S. P. Nolan and M. Szostak, A simple ¹H NMR method for determining the σ-donor properties of N-heterocyclic carbenes, *Tetrahedron Lett.*, 2019, **60**, 378–381.

47 G. Meng, L. Kakalis, S. P. Nolan and M. Szostak, A simple ¹H NMR method for determining the σ-donor properties of N-heterocyclic carbenes, *Tetrahedron Lett.*, 2019, **60**(4), 378–381.

48 M. Jabłoński, Halogen Bond to Experimentally Significant N-Heterocyclic (I, IMe2, IiPr2, ItBu2, IPh2, IMes2, IDipp2, IAd2; I = Imidazol-2-ylidene), *Int. J. Mol. Sci.*, 2023, **24**, 9057.

49 S. J. Grabowski, Halogen bonds with carbenes acting as Lewis base units: complexes of imidazol-2-ylidene: theoretical analysis and experimental evidence, *Phys. Chem. Chem. Phys.*, 2023, **25**, 9636–9647.

50 A. Y. Chernenko, V. A. Baydikova, V. V. Kutyrev, A. V. Astakhov, M. E. Minyaev, V. M. Chernyshev and V. P. Ananikov, Base–Ionizable Anionic NHC Ligands in Pd–catalyzed Reactions of Aryl Chlorides, *ChemCatChem*, 2024, **16**, e202301471.

51 A. Liske, K. Verlinden, H. Buhl, K. Schaper and C. Ganter, Determining the π-acceptor properties of N-heterocyclic carbenes by measuring the ⁷⁷Se NMR chemical shifts of their selenium adducts, *Organometallics*, 2013, **32**, 5269–5272.

52 K. Verlinden, H. Buhl, W. Frank and C. Ganter, Determining the Ligand Properties of N-Heterocyclic Carbenes from ⁷⁷Se NMR Parameters, *Eur. J. Inorg. Chem.*, 2015, **14**, 2416–2425.

53 C. H. Lee, D. A. Lutterman and D. G. Nocera, Photoactivation of metal-halogen bonds in a Ni(II) NHC complex, *Dalton Trans.*, 2013, **42**, 2355–2357.

54 C. M. Cardona, W. Li, A. E. Kaifer, D. Stockdale and G. C. Bazan, Electrochemical Considerations for Determining Absolute Frontier Orbital Energy Levels of Conjugated Polymers for Solar Cell Applications, *Adv. Mater.*, 2011, **23**, 2367–2371.

55 V. P. Ananikov, N. V. Orlov and I. P. Beletskaya, Efficient and Convenient Synthesis of β-Vinyl Sulfides in Nickel-Catalyzed Regioselective Addition of Thiols to Terminal Alkynes under Solvent-Free Conditions, *Organometallics*, 2006, **25**(8), 1970–1977.

56 D. A. Malyshev, N. M. Scott, N. Marion, E. D. Stevens, V. P. Ananikov, I. P. Beletskaya and S. P. Nolan, Homogeneous Nickel Catalysts for the Selective Transfer of a Single Arylthio Group in the Catalytic Hydrothiolation of Alkynes, *Organometallics*, 2006, **25**, 4462–4470.

57 *CrysAlisPro. Versions 1.171.42 and 1.171.43. Rigaku Oxford Diffraction*, 2023.

58 G. M. Sheldrick, SHELXT - Integrated space-group and crystal-structure determination, *Acta Crystallogr., Sect. A: Found. Adv.*, 2015, **71**, 3–8.

59 G. M. Sheldrick, Crystal structure refinement with SHELXL, *Acta Crystallogr., Sect. C: Struct. Chem.*, 2015, **71**, 3–8.

60 O. V. Dolomanov, L. J. Bourhis, R. J. Gildea, J. A. K. Howard and H. Puschmann, OLEX2: a complete structure solution, refinement and analysis program, *J. Appl. Crystallogr.*, 2009, **42**, 339–341.